1

Synthesis of Mathematical Models Representing Bioheat Transport

K. KHANAFER AND K. VAFAI

CONTENTS

1.1 Introduction 1
1.1.1 Hyperthermia 2
1.1.2 Bioheat Transfer in the Human Eye 3
1.2 Thermal Models for Blood-Perfused Tissues 6
1.2.1 The Pennes Bioheat Equation 6
1.2.2 Wulff Continuum Model 7
1.2.3 Klinger Continuum Model 8
1.2.4 Continuum Model of Chen and Holmes (CH) 8
1.2.5 The Weinbaum, Jiji, and Lemons (WJL) Bioheat Equation Model 11
1.2.6 The Weinbaum-Jiji Bioheat Equation Model 12
1.3 Mathematical Modeling of Bioheat Equation Using Porous-Media Theory 13
1.3.1 Energy Equation 13
1.3.2 Mathematical Model of Velocity Field and Macromolecule Transport within the Arterial Wall and Arterial Lumen 18
1.3.2.1 Lumen 18
1.3.2.2 Endothelium and Internal Elastic Lamina 19
1.3.2.3 Intima and Media 20
1.4 Conclusions 20
References 24

1.1 INTRODUCTION

The application of computational methods in modeling biological systems has been a topic of interest for various physicians and engineers. This interest stems from the rapid advancement of computational technology. Many medical operations have sought the help of engineering methods to ascertain the safety and to

determine the risk levels involved in any surgery. Further, the accurate description of the thermal interaction between vasculature and tissues is essential for the advancement of medical technology in treating fatal diseases such as tumors and breast cancer. At present, mathematical models have been used significantly in the analysis of hyperthermia in treating tumors, cryosurgery, laser eye surgery, fetal-placental studies, and many other applications. For example, the success of hyperthermia treatment strongly depends on knowledge of the heat transfer processes in blood-perfused tissues. As such, accurate thermal modeling is essential for effective hyperthermia treatment.

1.1.1 Hyperthermia

Hyperthermia treatment has been demonstrated effective as a cancer therapy in recent years. Its objective is to raise the temperature of pathological tissues above cytotoxic temperatures (41°C to 45°C) without overexposing healthy tissues [1–4]. Conventional hyperthermia in conjunction with radiation has demonstrated increased effectiveness in the treatment of certain types of cancer, such as those of liver metastases (the spread of a disease from one organ or part to another noncontiguous organ or part) [5–7]. Uniform temperature distributions are significant to achieve and maintain during hyperthermia treatment [8] since the use of temperatures above 55°C may directly destroy tissues through thermal coagulation, as was illustrated by Beacco et al. [9]. For safety consideration in clinics, it is essential to ensure necrosis (the death of living cells or tissues) of the total tumor cells within the desired volume of treatment while minimizing the thermal damage to healthy tissues surrounding the tumor. Temperature variations, which may be associated with the mechanisms of heat removal by the body and inadequate heating technologies, are often heterogeneous, and can lead to an undesired heating of the tissues, hot spots, and potential burning.

An important source of temperature nonuniformity is the presence of large vessels entering the heated volume and carrying blood at a low systemic temperature (37°C). Blood flow is found to have a profound influence on the efficiency of thermal therapy treatment. The design of delivered power devices and numerous theoretical, experimental, and clinical studies have demonstrated that large blood vessels may produce localized cooling regions within heated tissues during hyperthermia treatment [10–15]. Thus, for process control, it is essential to obtain a temperature field of the entire treatment region in order to deliver an adequate amount of energy to the treatment target volume and raise its minimum temperature above 42°C, while controlling the temperatures in the normal tissue to prevent damage. Since it is important to determine accurately the temperature field over the entire affected region, many numerical and experimental methods have been developed to solve the bioheat equation. Tang et al. [16] and Dai et al. [17] developed a numerical method for obtaining an optimal temperature distribution in a triple-layered skin structure embedded with two countercurrent, multilevel blood vessels: an artery and a vein. The authors concluded that their results

could be useful for certain types of hyperthermia cancer treatments, such as for skin cancer.

He et al. [18] developed a two-dimensional (2D) finite element thermal model of a human breast with a tumor to study the variation of the blood perfusion rate and distribution of oxygen partial pressure (PO_2) in human tumors. Laser irradiation was used as an adjunct method in the treatment of cancer. The blood circulation inside the breast was modeled using one-dimensional nonlinear equations of pulsatile fluid flow. The distribution of PO_2 inside the capillaries, tumor vessels, and surrounding tissue was obtained by the Krogh analysis model (the Krogh model predicts a biphasic relationship between O_2 delivery and the rate of O_2 uptake per unit tissue volume). Shih et al. [19] used the explicit finite difference method to solve the transient equation for the temperature field within a perfused tumor tissue encompassing a blood vessel in an axisymmetric configuration during thermal therapy. Their results illustrated that short-duration high-intensity heating was more effective for treating a tumor with a blood vessel of 200 μm or less diameter, while neither longer heating duration nor higher heating power density was sufficient for complete necrosis of a tumor with a blood vessel with a diameter larger than 2 mm. Zhou and Liu [20] developed a three-dimensional (3D) time-dependent heat transfer model coupled with the Navier-Stokes equation-based blood flow model to solve for temperature distributions in laser-irradiated tissues embedded with large blood vessels and the flow field within the vessels. A better understanding of the role of a large vessel in laser-induced thermotherapy (LITT) was obtained.

Khanafer et al. [21] conducted a numerical study to determine the influence of pulsatile laminar flow and heating protocol on the temperature distribution in a single blood vessel and tumor tissue receiving hyperthermia treatment using physiological velocity waveforms. Their results showed that the presence of large vessels had a significant effect on temperature distributions. Further, a uniform heating scheme was found to generate larger temperatures compared to the pulsed heating scheme, which may induce areas of overheating (beyond the therapeutic regions) that could damage normal tissues (Figure 1.1).

Craciunescu and Clegg [22] analyzed the effects of pulsating blood flow on the temperature distribution of a heated tissue. They found that the pulsation of blood flow rate yields an obvious change of the energy transport between the vessel wall and the blood flow within large blood vessels. Their results were based on the assumption that the vessel wall was a perfect thermal sink.

1.1.2 Bioheat Transfer in the Human Eye

With the growing interest in the bioengineering field, the area of ophthalmology, in particular laser eye surgery, has become better known in the last 20 years [23]. This field has gained increasing popularity with the advancement of computational technology. The popular employment of laser technology for surgical applications has given rise to a new area of burn studies, that is, the change in

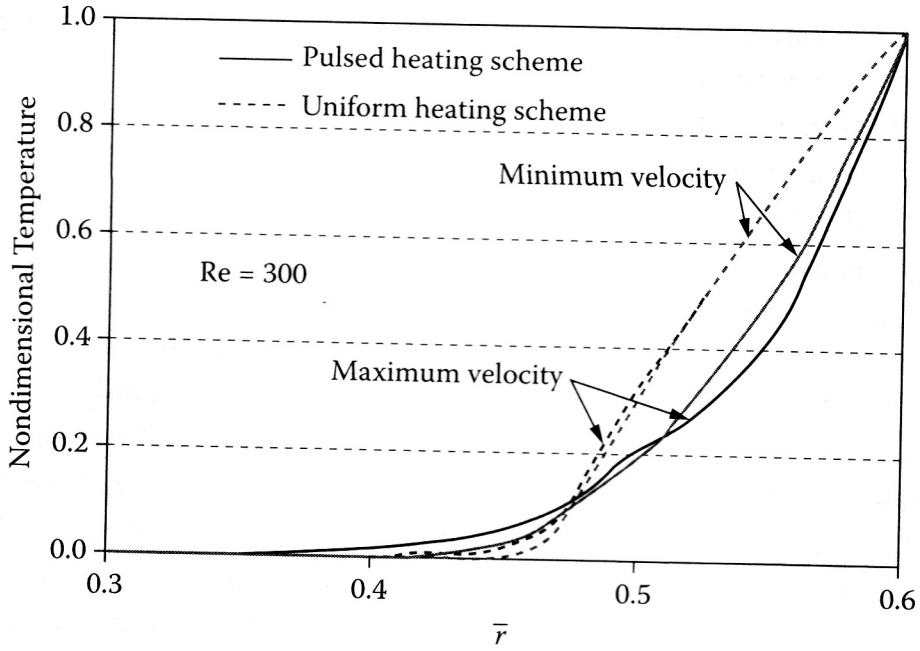

Figure 1.1 Influence of the heating protocol on the temperature distribution at various flow conditions. (Reprinted from Khanafer et al. [21]. With permission from Elsevier.)

temperature of the bio-organ associated with the absorption of high-intensity irradiation of light. As early as the 1960s, when lasers were first introduced in the medical field, there was immediate concern over the potential of incurring injury to the eye owing to the absorption of energy causing elevated temperatures. Injury to the eye can be severe when the blood flow cannot regulate the heat loading within the ocular tissues. The tissues most vulnerable in the eye are the cornea and the aqueous humor, as the infrared radiation raises the overall temperature of the aqueous eye [23,24]. Invasive or direct-contact techniques initially used in measuring the eye temperature are now confined to animal experiments due to the damaging nature of the test procedures [25]. The application of military technology in medical sciences has a way for measuring human body temperature utilizing infrared imaging. Infrared (IR)-imaging techniques have been widely used in measuring the temperature of the eye ever since. The human eye is very sensitive, and any direct contact with foreign objects is intolerable. Computational modeling of the human eye is thus very important for estimating the eye temperature during an eye procedure. A mathematical model can be useful for the doctors in enabling them to optimize their surgical protocol. This will lead to a reduction in intraocular tissue thermal damage.

Ooi et al. [26] used the boundary element method to analyze the 2D steady-state bioheat model of the human eye. The human eye was modeled as comprising four distinct homogeneous regions. The boundary condition on the outer surface of the cornea was nonlinear due to heat radiation. An iterative approach was used to treat the nonlinear heat radiation term. The authors showed that the calculated heat flux results were more accurately obtained using the boundary element method than the finite element method on the corneal surface. Ng and

Ooi [27] developed a 2D finite element model to simulate the thermal steady-state conditions of the human eye based on the properties and parameters reported in the open literature. Their results were verified against previous studies on human as well as animal eyes. Their results compared favorably with images from IR screening and another finite element model. Extending earlier work, Ng and Ooi [28] also developed a 3D model of the human eye to simulate the steady-state temperature distribution during standard conditions and during electromagnetic (EM) wave radiation. Their results were in good agreement with the experimental results in the open literature.

A mathematical model of the human eye based on the bioheat transfer equation was developed by Scott [29]. The intraocular temperature distribution was calculated using the Galerkin finite element method. A mathematical model to predict the temperature distribution within the human eye when subjected to a laser source was presented by Chuak et al. [30]. The model was developed by employing the Pennes bioheat transfer equation. The intraocular temperature distributions were calculated using the finite volume method. To compute the intraocular temperature distribution, Amara [31] presented a thermal model of the human eye exposed to laser irradiation. The physical system was described by a set of partial differential equations consisting of the heat equation that included the laser heat source, and the boundary and initial conditions. The analytical system was transformed to an integral formulation where a Galerkin function was applied. The results illustrated that decreasing the laser wavelength increases the adverse effects on the eye. This was due to the production of higher temperatures that can lead to the denaturation of the ocular tissues.

Long-term industrial exposure to low levels of infrared radiation has for many years been associated with the development of cataracts, which is considered to be a thermally related injury. A finite element model of the human eye was employed to calculate the temperature rise experienced by the intraocular media when exposed to infrared radiation [32]. The model was used to calculate transient and steady-state temperature distributions for various exposure times and a range of incident irradiances. The effect of the eye's natural cooling mechanisms on the heating was investigated. Hirata et al. [33–35] applied the finite difference time domain method to study the temperature rise in the human eye exposed to electromagnetic waves. Hirata [33] investigated the effect of frequency, polarization, and angle of incidence of an electromagnetic (EM) wave on the specific absorption rate (SAR) and maximum temperature increase in the human eye at 900 MHz, 1.5 GHz, and 1.9 GHz. In particular, the temperature increase in the eye was compared for near-field and far-field exposures. The results illustrated that the SAR and temperature increase in the eye were found to be largely dependent on the separation between the eye and a source, and the frequency, polarization, and angle of incidence of the EM wave. Lagendijk [36] conducted measurements on rabbit eyes and used the results to predict the thermal properties of the rabbit eye using a finite difference method. The measured temperature at the cornea

surface was in good agreement with the calculated temperature using the finite difference method (FDM) mathematical model at the same location.

1.2 THERMAL MODELS FOR BLOOD-PERFUSED TISSUES

Heat transport in biological tissues, which is usually expressed by the bioheat equation, is a complicated process since it involves thermal conduction in tissues, convection and perfusion of blood (delivery of the arterial blood to a capillary bed in tissues), and metabolic heat generation. Therefore, several authors have developed mathematical models of bioheat transfer as extended and modified versions of the original work of Pennes [37], as reported by Charny [38] and Arkin et al. [39]. An example of the applications of the bioheat equation exists in the fetal-placental studies. The existence of a thermal gradient between fetal and maternal tissue has been considered a medical subject of research interest. This gradient is found to play a significant role in dissipating heat produced by the fetus during its metabolic processes. The magnitude of this temperature difference is determined by the fetal metabolic rate and the rate of heat exchange from fetal to maternal tissues [40–46].

Another example of the bioheat equation is related to the presence of the global system mobile (GSM) electromagnetic fields in the environment due to cellular phones and base stations, which have been causing increasing public concern regarding the possible adverse health effects of these fields. Electromagnetic-thermal analysis of human exposure to base station antenna radiation was presented by Poljak et al. [47]. The formulation was based on a simplified cylindrical representation of the human body. The electromagnetic analysis involved incident and internal field dosimetry, while the thermal model was based on the Pennes bioheat transfer equation for solving thermal processes inside the human body. In what follows, a concise summary of the pertinent thermal models and their limitations for blood-perfused tissues that best categorize different approaches in modeling the bioheat transfer is presented.

1.2.1 The Pennes Bioheat Equation

The Pennes model [37] was initially developed for predicting heat transfer in the human forearm. Due to the simplicity of the Pennes bioheat model (it assumes uniform thermal conductivity, perfusion rate, and metabolic heating), it was implemented in various biological research works such as for therapeutic hyperthermia for the treatment of cancer [48–50]. The equation that Pennes developed is expressed in its simplest form as

$$(\rho c_p)_t \frac{\partial T_t}{\partial t} = \nabla \cdot (k_t \nabla T_t) + q_p + q_m \tag{1.1}$$

where ρ, c_p, T_t, k_t, and q_m are tissue density, tissue-specific heat, tissue temperature, tissue thermal conductivity, and uniform rate of metabolic heat generation in the tissue layer per unit volume, respectively. The heat transfer from the blood to the tissue, q_p, is assumed to be proportional to the temperature difference between the arterial blood entering the tissue and the venous blood leaving the tissue. This quantity is presented as

$$q_p = \omega \rho_b c_b (T_{a,in} - T_{v,out}) \tag{1.2}$$

where $T_{a,in}$ and $T_{v,out}$ are the temperature of the blood upon entering and leaving the tissue via the arteriole–venule network, respectively; ρ_b is the blood density; c_b is the blood-specific heat; and ω is the volumetric rate of blood perfusion in the tissue per unit volume. The Pennes model assumed thermal equilibrium between the venous blood and the tissue temperatures (i.e., $T_{v,out} = T_t$), yielding the familiar Pennes perfusion heat source term:

$$q_p = \omega \rho_b c_b (T_{a,in} - T_t) \tag{1.3}$$

1.2.2 Wulff Continuum Model

Due to the simplicity of the Pennes model, many authors have looked into the validity of the assumptions used to develop the Pennes bioheat equation. Wulff's study [51] was one of the first that questioned the assumptions of the Pennes model. Wulff [51] assumed that the heat transfer between flowing blood and tissue should be modeled to be proportional to the temperature difference between these two media rather than between the two bloodstream temperatures (i.e., the temperature of the blood entering and leaving the tissue). Thus, the energy flux at any point in the tissue should be expressed by

$$q = -k_t \nabla T_t + \rho_b h_b \mathrm{v}_h \tag{1.4}$$

where v_h is the local mean blood velocity and T_t is the tissue temperature. The specific enthalpy of the blood h_b, which accounts for both the sensible enthalpy plus the enthalpy of reaction, is given by

$$h_b = \int_{T_o}^{T_b} c_b(T_b^*) dT_b^* + \frac{P}{\rho_b} + \Delta H_f (1 - \phi) \tag{1.5}$$

where P is the system pressure, ΔH_f is the enthalpy of formation of the metabolic reaction, and ϕ is the extent of reaction, respectively. T_o and T_b are the

reference and blood temperatures, respectively. Thus, the energy balance equation can be written as

$$\rho c_p \frac{\partial T_t}{\partial t} = -\nabla \bullet q = -\nabla \bullet (-k_t \nabla T_t + \rho_b h_b \mathrm{v}_h) = \nabla \bullet \left[k_t \nabla T_t - \rho_b \mathrm{v}_h \left(\int_{T_o}^{T_b} c_b (T_b^*) dT_b^* + \frac{P}{\rho_b} + \Delta H_f (1-\phi) \right) \right] \tag{1.6}$$

Neglecting the mechanical work term (P/ρ_b), setting the divergence of the product $(\rho_b \mathrm{v}_h)$ to zero, and assuming constant physical properties, Equation (1.6) can be simplified as follows:

$$\rho c_p \frac{\partial T_t}{\partial t} = k_t \nabla^2 T_t - \rho_b \mathrm{v}_h (c_b \nabla T_b - \Delta H_f \nabla \phi) \tag{1.7}$$

Since blood is effectively microcirculating within the tissue, it will likely be in thermal equilibrium with the surrounding tissue. As such, Wulff [51] assumed that T_b is equivalent to the tissue temperature T_t. The metabolic reaction term $(\rho_b \mathrm{v}_h \Delta H_f \nabla \phi)$ is equivalent to q_m; therefore, the final form of the bioheat equation that was derived by Wulff [51] is

$$(\rho c_p)_t \frac{\partial T_t}{\partial t} = k_t \nabla^2 T_t - (\rho c)_b \mathrm{v}_h \bullet \nabla T_t + q_m \tag{1.8}$$

The main challenge in solving this bioheat equation is in the evaluation of the local blood mass flux $\rho_b \mathrm{v}_h$.

1.2.3 Klinger Continuum Model

Since the Pennes model [37] neglected the effect of blood flow inside the tissues, Klinger [52] considered the convective heat transfer caused by the blood flow inside the tissue. Taking into account the spatial and temporal variations of the velocity (v) and heat source, and assuming constant physical properties of tissue and incompressible blood flow, the modified Pennes model was expressed as

$$(\rho c_p)_t \frac{\partial T_t}{\partial t} + (\rho c)_b \mathbf{v} \bullet \nabla T_t = k_t \nabla^2 T_t + q_m \tag{1.9}$$

1.2.4 Continuum Model of Chen and Holmes (CH)

Similar to the analysis of Wulff [51] and Klinger [52], the bioheat transfer analysis of Chen and Holmes [53] is a microvascular model. The Chen and Holmes

(CH) model [53] assumes that the total tissue control volume is composed of the solid-tissue subvolume (V_s) and blood subvolume (V_b). Using a simplified volume-averaging technique, the energy balance equations for both the solid-tissue space and vascular spaces can be written as follows:

Solid Phase

$$\delta V_s(\rho c)_s \frac{\partial T_s}{\partial t} = dQ_{ks} + dQ_{bs} + dQ_m \tag{1.10}$$

where ρ_s and c_s are the solid-tissue density and specific heat, respectively; δV_s is the differential volume of the solid phase; dQ_{ks} is the energy transferred by conduction; dQ_{bs} is the heat gain from the blood subvolume; and dQ_m is the metabolic heating energy.

The energy balance equation for the vascular space is similar to Equation (1.10) except with an additional term associated with the bulk fluid flow in this space:

Fluid Phase

$$\delta V_b(\rho c)_b \frac{\partial T_b}{\partial t} = dQ_{kb} - dQ_{bs} + \int_S (\rho c)_b T\mathbf{v} \bullet d\mathbf{s} \tag{1.11}$$

where ρ_b and c_b are the blood density and specific heat, respectively; δV_b is the differential volume of the blood in the vascular space; dQ_{kb} is the conductive contribution; and the integral term in Equation (1.11) denotes the energy transfer by convection as the blood flows across the surface area S at velocity $\mathbf{v}$. Therefore, the energy balance for the tissue space is derived by the addition of Equations (1.10) and (1.11) and division of the result by the total control volume δV, which yields the following:

$$(\rho c)\frac{\partial T_t}{\partial t} = q_k + q_m + q_p \tag{1.12}$$

where ρ and c are

$$\rho = (1-\varepsilon_b)\rho_s + \varepsilon_b\rho_b \quad \text{and} \quad c = \frac{1}{\rho}[(1-\varepsilon_b)\rho_s c_s + \varepsilon_b\rho_b c_b] \tag{1.13}$$

where ε_b is the porosity of the tissue where blood flows and T_t is the local mean tissue temperature expressed as

$$T_t = \frac{1}{\rho c}[(1-\varepsilon_b)(\rho c)_s T_s + \varepsilon_b(\rho c)_b T_b] \tag{1.14}$$

The quantity q_k denotes the heat transfer by conduction per unit volume, q_m is the metabolic heat generation per unit volume, and q_p is the perfusion energy

generated per unit volume. The total heat transfer by conduction per unit volume (q_k) in the tissue control volume is expressed by

$$q_k = \frac{Q_{ks} + Q_{kb}}{\delta V} = \nabla \bullet (k_{eff} \nabla T_t) \tag{1.15}$$

where k_{eff} is the effective thermal conductivity of the combined tissue and vascular spaces. The effective thermal conductivity is written as

$$k_{eff} = \varepsilon_b k_b + (1 - \varepsilon_b) k_s \tag{1.16}$$

Since $\varepsilon_b = \frac{\delta V_b}{\delta V} \sim \frac{\delta V_b}{\delta V_s} << 1$, it follows that k_{eff} is independent of blood flow and equal to the conductivity of the solid tissue ($k_{eff} \cong k_s$).

In Wulff's formulation [51], thermal equilibrium was assumed between blood and the solid-tissue medium at all locations within the control volume. However, Chen and Holmes [53] allowed for the blood within the tissue matrix to flow at a temperature different than the tissue temperature. Therefore, the convective heat transfer across the surface (q_p) due to blood flow was written as the sum of the perfusion heating term (originated by Pennes), a contribution proportional to local blood perfusion velocity as represented by the Wulff model [51], and a contribution due to the perfusion thermal conductivity. Thus, the perfusion term including all these terms is

$$q_p = \frac{1}{\delta V} \int_S \rho_b c_b T \mathbf{v} \bullet ds \cong (\rho c)_b \omega^* (T_a^* - T_s) - (\rho c)_b \mathbf{v}_p \bullet \nabla T_s + \nabla \bullet k_p \nabla T_s \tag{1.17}$$

where $\mathbf{v}_p$ is the mean perfusion velocity; ω^* is the total perfusion bleed-off to the tissue only from the microvessels, while the Pennes term ω includes bleed-off from all generations of the vasculature; T_a^* is the blood temperature; and T_s is the solid-tissue temperature. Note that T_a^* is different from T_a (temperature of blood entering the tissue), which was used in the Pennes model; see Equation (1.2). The second term in Equation (1.17) is indicative of blood convective perfusion, and the third term on the right-hand side of Equation (1.17) indicates the enhancement of thermal conductivity in a tissue due to the blood flow within microvessels (i.e., the thermal dispersion effect).

Therefore, the bioheat equation based on the Chen and Holmes [53] model can be written as

$$(\rho c_p)_t \frac{\partial T_t}{\partial t} = \nabla \bullet (k_{eff} \nabla T_t) + (\rho c)_b \omega^* (T_a^* - T_t) - (\rho c)_b \mathbf{v}_p \bullet \nabla T_t + \nabla \bullet k_p \nabla T_t + q_m \tag{1.18}$$

where T_s is replaced by the volume-weighted continuum temperature (T_t). This is reasonable as long as $\varepsilon_b << 1$.

1.2.5 The Weinbaum, Jiji, and Lemons (WJL) Bioheat Equation Model

Weinbaum and colleagues [54–56] modified the thermal conductivity in the Pennes equation by means of an "effective conductivity," which is a function of the blood flow rate and vascular geometry. The modified bioheat equation was obtained based on a hypothesis that small arteries and veins are parallel and the flow direction is countercurrent, resulting in counterbalanced heating and cooling effects. It should be noted that this assumption is mainly applicable within the intermediate tissue of the skin. Neglecting axial conduction, the artery and vein energy balances are written as

$$(\rho c)_b \frac{d}{ds}\left(n\pi a^2 \bar{u} T_a\right) = -nq_a - (\rho c)_b (2\pi a n g) T_a \tag{1.19}$$

$$(\rho c)_b \frac{d}{ds}\left(n\pi a^2 \bar{u} T_v\right) = -nq_v - (\rho c)_b (2\pi a n g) T_v \tag{1.20}$$

where q_a is the heat loss from the artery by conduction through its wall, q_v is the heat gain by conduction per unit length through the vein wall into the vein, T_a and T_v are the bulk mean temperatures inside the blood vessel, n is the number of arteries or veins, $\bar{u}$ is the mean velocity in either the artery or vein, a is the radius, and g is the perfusion bleed-off velocity per unit vessel surface area. The second term on the right-hand side of Equation (1.19) indicates heat loss from the arterial blood due to perfusion bleed-off, while in Equation (1.20) it represents the heat gain by the venous blood from perfusion drainage. For an equal-size artery–vein pair, subtracting Equation (1.20) from Equation (1.19) yields

$$(\rho c)_b \left[\frac{d}{ds}\left(n\pi a^2 \bar{u} T_a\right) - \frac{d}{ds}\left(n\pi a^2 \bar{u} T_v\right)\right] = -n(q_a - q_v) - (\rho c)_b (2\pi a n g)(T_a - T_v) \tag{1.21}$$

where the first term on the right-hand side is the net heat transfer by conduction from the tissue into the paired vessels, and the second term is the net heat deposited in the tissue due to the perfusion bleed-off. The first term on the left-hand side represents the total blood heat exchange in the countercurrent vessels and the surrounding tissue. This term can be balanced by conduction and metabolic heating as follows:

$$(\rho c)_b \left[\frac{d}{ds}\left(n\pi a^2 \bar{u} T_a\right) - \frac{d}{ds}\left(n\pi a^2 \bar{u} T_v\right)\right] = \nabla \bullet (k_t \nabla T_t) + q_m \tag{1.22}$$

If the continuity equation $\left[\frac{d}{ds}(na^2\bar{u}) = -2nag\right]$ is used, the second terms in the right-hand side of Equations (1.19) and (1.20) can be eliminated, yielding the

following equations:

$$q_a = -(\rho c)_b(\pi a^2 \bar{u})\frac{dT_a}{ds} \;\&\; q_v = -(\rho c)_b(\pi a^2 \bar{u})\frac{dT_v}{ds} \tag{1.23}$$

Therefore, the rate of the energy entering and leaving the tissue control volume can be expressed as

$$q_a - q_v = (\rho c)_b(\pi a^2 \bar{u})\frac{d}{ds}[T_v - T_a] \tag{1.24}$$

Thus, the final form of the bioheat equation can be obtained by substituting Equation (1.22) for the left-hand side of Equation (1.21) and substituting Equation (1.24) for the first term on the right-hand side of Equation (1.21) as

$$(\rho c)_b(n\pi a^2 \bar{u})\frac{d}{ds}[T_a - T_v] - (\rho c)_b(n2\pi a\, g)(T_a - T_v) = \nabla \bullet (k_t \nabla T_t) + q_m \tag{1.25a}$$

or

$$(\rho c)_b(n\pi a^2 \bar{u})\frac{d}{ds}[T_a - T_v] = \nabla \bullet (k_t \nabla T_t) + (\rho c)_b \omega'(T_a - T_v) + q_m \tag{1.25b}$$

where $\omega' = (n2\pi a\, g)$. Equation (1.25) includes a perfusion bleed-off term that apparently resembles the Pennes perfusion term. This term is proportional to $(T_a - T_v)$ rather than $(T_a - T_t)$.

1.2.6 The Weinbaum-Jiji Bioheat Equation Model

Since both T_a and T_v are unknowns in Equation (1.23), the tissue temperature T_t cannot be determined. Therefore, Weinbaum and Jiji [57] derived a simplified single equation to study the influence of blood flow on the tissue temperature distribution. The mean tissue temperature can be approximated as

$$T_t \cong \frac{T_a + T_v}{2} \tag{1.26}$$

Thus, the magnitude of the difference $(q_a - q_v)$ is much smaller than the magnitude of either q_a or q_v. Moreover, Weinbaum and Jiji [57] assumed that the tissue surrounding the vessel pair is a pure conduction region such that

$$q_a \cong q_v = \sigma k_t (T_a - T_v) \tag{1.27}$$

where σ is a geometrical shape factor given by

$$\sigma = \frac{\pi}{\cosh^{-1}(L_s/a)} \tag{1.28}$$

The ratio (L_s/a) indicates the ratio of the vessel spacing to vessel diameter. Equations (1.23), (1.26), and (1.27) are solved to obtain an equation for the artery–vein temperature difference and the tissue temperature gradient by adding the q_a and q_v terms from Equation (1.23):

$$T_a - T_v = -\frac{\pi a^2 \bar{u} (\rho c)_b}{\sigma k_t} \frac{dT_t}{ds} \tag{1.29}$$

Substituting Equation (1.29) in the original WJL model, Equation (1.25a), yields a new bioheat equation proposed by Weinbaum and Jiji [57] as follows:

$$\frac{n\pi^2 a k_b}{4k_t} Pe \left(\frac{2gPe}{\sigma \bar{u}} \frac{dT_t}{ds} - \frac{d}{ds}\left[\frac{aPe}{\sigma} \frac{dT_t}{ds} \right] \right) = \nabla \bullet (k_t \nabla T_t) + q_m \tag{1.30}$$

where Pe is the Peclet number; which is defined as $Pe = \frac{2a(\rho c)_b \bar{u}}{k_b}$.

Table 1.1 illustrates a summary of variants within the previously discussed models.

1.3 MATHEMATICAL MODELING OF BIOHEAT EQUATION USING POROUS-MEDIA THEORY

1.3.1 Energy Equation

Although Pennes's bioheat equation is considered to be a useful model to predict temperature distribution in the human body due to its simplicity, it is still questionable. Based on the previous section, one can note that the summarized bioheat transfer models in Table 1.1 are extended or modified versions of the original work of Pennes's model. They were based on improving the main flaws of Pennes's equation. An accurate description of the thermal interaction between vasculature and tissues is essential for the advancement of medical technology through effective modeling of arteries, tissues, and organs. Therefore, it is crucial to develop a more robust bioheat model that incorporates the effects of blood thermal dispersion, porosity variation, effective tissue conductivity, and effective tissue capacitance, and a more precise representation of the heat exchange between the blood and the tissue. Since the compound matrix of tissues, arteries, veins, and capillary tubes can be considered as a porous medium, porous media theory is very well suitable for developing a rigorous model of a bioheat equation.

Transport phenomena in porous media have received continuing interest in the past five decades. This interest stems from their importance in many industrial and clinical applications [58–60]. Examples include computational biology, tissue replacement production, drug delivery, advanced medical imaging, porous scaffolds for tissue engineering, and transport in biological tissues [61–65]. Porous media theory may also be utilized in biosensing systems [66–69]. Some aspects of transport in porous media were also discussed in the

Table 1.1 Analysis of Variants within Bioheat Transfer Models

Model	Transient Term	Conduction Term	Perfusion Term	Metabolic Heat Source
General[a]	$(\rho c_p)_t \frac{\partial T_t}{\partial t}$	$\nabla \bullet (k_{eff} \nabla T_t)$	q_p	q_m
Pennes	$(\rho c_p)_t \frac{\partial T_t}{\partial t}$	$k_t \nabla^2 T_t$	$(\rho c)_b \omega (T_{a,in} - T_{v,out})$	q_m
Wulff	$(\rho c_p)_t \frac{\partial T_t}{\partial t}$	$k_t \nabla^2 T_t$	$-(\rho c)_b v_h \nabla T_t$	$\rho_b v_h \Delta H_f \nabla \phi$
Klinger	$(\rho c_p)_t \frac{\partial T_t}{\partial t}$	$k_t \nabla^2 T_t$	$-(\rho c)_b \mathbf{v} \nabla T_t$	q_m
Chen and Holmes	$(\rho c_p)_t \frac{\partial T_t}{\partial t}$	$\nabla \bullet (k_{eff} \nabla T_t)$	$-(\rho c)_b \mathbf{v}_p \bullet \nabla T_t + (\rho c)_b \omega^* (T_a^* - T_t) + \nabla \bullet (k_p \nabla T_t)$	q_m
Weinbaum, Jiji, and Lemons	NA	$\nabla \bullet (k_t \nabla T_t)$	$(\rho c)_b (n 2\pi a\, g)(T_a - T_v) - (\rho c)_b (n\pi a^2 \bar{u}) \frac{d}{ds}[T_a - T_v]$	q_m
Weinbaum and Jiji	NA	$\nabla \bullet (k_t \nabla T_t)$	$\frac{n\pi^2 a k_b}{4k_t} Pe \left(-\frac{2gPe}{\sigma \bar{u}} \frac{dT_t}{ds} + \frac{d}{ds}\left[\frac{aPe}{\sigma} \frac{dT_t}{ds} \right] \right)$	q_m

[a] $(\rho c_p)_t \frac{\partial T_t}{\partial t} = \nabla \bullet (k_{eff} \nabla T_t) + q_p + q_m$.

two editions of the *Handbook of Porous Media* [69,70] and in Hadim and Vafai [71] and Vafai and Hadim [72]. Complicated and interesting biomedical aspects can be modeled using the porous media concept. Xuan and Roetzel [73,74] utilized the porous media approach to model a tissue–blood system composed mainly of tissue cells and interconnected voids that contain either arterial or venous blood. The thermal energy exchange between the tissue and blood was modeled using the principle of local thermal nonequilibrium as described in the works of Amiri and Vafai [75,76]; Alazmi and Vafai [77]; Lee and Vafai [78]; Vafai and Sozen [79–81]; and Sozen and Vafai [82,83]. Thus, two energy equations were derived that represent the blood phase and the solid matrix phase, as given below:

Blood Phase

$$\varepsilon(\rho c)_b\left(\frac{\partial <T>^b}{\partial t}+<\vec{V}>^b\cdot\nabla <T>^b\right)=\nabla\cdot\left(\mathbf{k}_b^a\cdot\nabla <T>^b\right)+h_{bs}[<T>^s-<T>^b] \tag{1.31}$$

Solid Matrix Phase

$$(1-\varepsilon)(\rho c)_s\frac{\partial <T>^s}{\partial t}=\nabla\cdot\left(\mathbf{k}_s^a\cdot\nabla <T>^s\right)-h_{bs}[<T>^s-<T>^b]+(1-\varepsilon)q_m \tag{1.32}$$

where $<T>^b, <T>^s, \mathbf{k}_b^a, \mathbf{k}_s^a, <\vec{V}>^{\mathbf{b}}$ and h_{bs}, and ε are the local volume-averaged arterial blood temperature, local volume-averaged solid-tissue temperature, blood effective thermal conductivity tensor, solid-tissue effective thermal conductivity tensor, blood velocity vector, and interstitial convective heat transfer coefficient, respectively. The interstitial convective heat transfer coefficient is a function of blood velocity and properties and geometric structure of the solid phase. The heat exchange between the blood and the tissue is expressed as $h_{bs}[<T>^s-<T>^b]$. For isotropic conduction, the effective thermal conductivity $\mathbf{k}_b^a$ of blood and solid tissue $\mathbf{k}_s^a$ can be expressed as

$$\mathbf{k}_b^a=\varepsilon\boldsymbol{k}_b+\boldsymbol{k}_b^t \quad \text{and} \quad \mathbf{k}_s^a=(1-\varepsilon)\boldsymbol{k}_s \tag{1.33}$$

where $\boldsymbol{k}_b^t$ is the thermal dispersion conductivity. The concept of thermal dispersion is well established in the theory of porous media as presented in the works of Amiri and Vafai [75,76]. Due to insufficient knowledge about the thermal and anatomic properties of tissue, the velocity field of the blood, and interstitial convective heat transfer coefficients, the local thermal equilibrium model represents a good approximation for determining the temperature field in applications involving small-sized blood vessels ($\varepsilon << 1$). This implies that blood flowing in these small vessels will be completely equilibrated with the surrounding tissue.

Therefore, Equations (1.31) and (1.32) reduce to the following equation [21,85]:

$$\left[(\rho c)_b \varepsilon + (1-\varepsilon)(\rho c)_s\right]\frac{\partial <T>}{\partial t} + \varepsilon(\rho c)_b <\vec{V}>^b \cdot \nabla <T> = \nabla\left[\left(\mathbf{k}_s^a + \mathbf{k}_b^a\right)\cdot \nabla <T>\right] + q_m(1-\varepsilon) \tag{1.34}$$

The second term on the left-hand side of Equation (1.34) represents the heat transfer due to the blood perfusion. Note that the perfusion source term in the Pennes model was derived based on a uniform blood perfusion assumption and was equal to $\omega\rho_b c_b(T_{a,in} - T_{v,out})$. The representation of the blood perfusion in Equation (1.34) is more consistent with representation in the Klinger and Wulff models. In hyperthermia applications, tissue may absorb energy from an external source such as electromagnetic or ultrasonic radiation, and, therefore, another heat source term should be added to the right side of Equation (1.34) as follows:

$$[(\rho c)_b \varepsilon + (1-\varepsilon)(\rho c)_s]\frac{\partial <T>}{\partial t} + \varepsilon(\rho c)_b <\vec{V}>^b \cdot \nabla <T> = \nabla\left[\left(\mathbf{k}_s^a + \mathbf{k}_b^a\right)\cdot \nabla <T>\right] + q_m(1-\varepsilon) + q_h(1-\varepsilon) \tag{1.35}$$

Table 1.2 and Table 1.3 summarize the previously discussed bioheat transfer models in this work.

Table 1.2 Main Characteristics of Bioheat Models Using the Porous Media Approach

Bioheat Model	Main Characteristics
Porous media model (local thermal equilibrium principle)[a]	This model modifies the Pennes equation by accounting for the following effects: Variable tissue porosity Effective tissue conductivity Effective tissue capacitance Blood dispersion
Porous media model (local thermal nonequilibrium principle)[b]	This model requires more knowledge about the thermal and anatomic properties of the tissue, the velocity field of the blood, and interstitial convective heat transfer coefficients. This model considers the following effects: Variable tissue porosity Blood dispersion Effective tissue conductivity Effective tissue capacitance

[a] Amiri and Vafai [75,76]; Marafie and Vafai [84].

[b] Amiri and Vafai [75,76]; Alazmi and Vafai [77]; Lee and Vafai [78]; Vafai and Sozen [79–81]; Sozen and Vafai [82,83].

Table 1.3 Main Characteristics of Bioheat Models Using a Simplified Approach

Bioheat Model	Assumptions	Main Characteristics
Pennes [37]	Uniform physical properties and metabolic heating Heat transfer from the blood to the tissue is proportional to the temperature difference between the arterial blood entering the tissue and the venous blood leaving the tissue	Simple model Not valid for all tissues
Wulff [51]	Thermal equilibrium between flowing blood and the surrounding tissue Uniform mean blood velocity inside the tissue	Modified version of the Pennes model
Klinger [52]	Constant physical properties	Considers the convective heat transfer caused by the blood flow inside the tissue Considers the spatial and temporal variations of the velocity field and heat source
Chen and Holmes [53]	Utilized two separate volumes: one for solid tissue and one for blood in the vascular space	The total heat transfer by conduction relates to heat transfer by conduction in the solid tissue and in the vascular space The total perfusion term corresponds to the effect of blood flow on tissue temperature around large vessels, heat transfer that takes place as a result of the blood flow, and heat transfer due to the small temperature changes (microvessels) Introduce perfusion conductivity tensor in the bioheat equation. Allows for the blood within the tissue matrix to flow at a temperature different than that of the tissue temperature

(*Continued*)

Table 1.3 Main Characteristics of Bioheat Models Using a Simplified Approach (Continued)

Bioheat Model	Assumptions	Main Characteristics
Weinbaum, Jiji, and Lemons [54–56]	Based on a hypothesis that small arteries and veins are parallel and the flow direction is countercurrent, resulting in counterbalanced heating and cooling effects	Coupled energy equations for artery–vein pair and tissue
	Isotropic blood perfusion between the countercurrent vessels	Utilizes the effective conductivity
Weinbaum and Jiji [57]	The mean tissue temperature is approximated by an average temperature of the bulk mean temperatures inside the blood vessel	Valid when arteries and veins are close, leading to negligible blood perfusion effects
	Assumes that the tissue around the vessel pair is a pure conduction region	Utilizes the effective conductivity

1.3.2 Mathematical Model of Velocity Field and Macromolecule Transport within the Arterial Wall and Arterial Lumen

In order to solve Equations (1.31), (1.34), and (1.35), the velocity distribution within a tissue should be determined first. Khanafer et al. [21] modeled the arterial wall as a homogeneous porous medium. The velocity distribution within the tissue was determined using the volume-averaged governing equations of porous media coupled with the velocity field in the blood vessel. Vafai and coworkers [61–65] had developed a new fundamental and comprehensive four-layer model for the description of the velocity field and mass transport in the arterial wall coupled with the velocity field and mass transport in the arterial lumen. The endothelium, intima, internal elastic lamina (IEL), and media layers were all treated as macroscopically homogeneous porous media and mathematically modeled using proper types of the volume-averaged porous media equations, with the Staverman filtration and osmotic reflection coefficients employed to account for selective permeability of each porous layer to certain solutes. The typical anatomical structure of an arterial wall is shown schematically in Figure 1.2.

1.3.2.1 Lumen

Assuming incompressible and Newtonian fluid flow, blood flow in the arterial lumen was modeled using Navier-Stokes and continuity equations as follows:

$$\nabla \cdot \vec{V} = 0 \tag{1.36}$$

$$\frac{\partial \vec{V}}{\partial t} + \vec{V} \cdot \nabla \vec{V} = -\frac{1}{\rho} \nabla P + \nu \nabla^2 \vec{V} \tag{1.37}$$

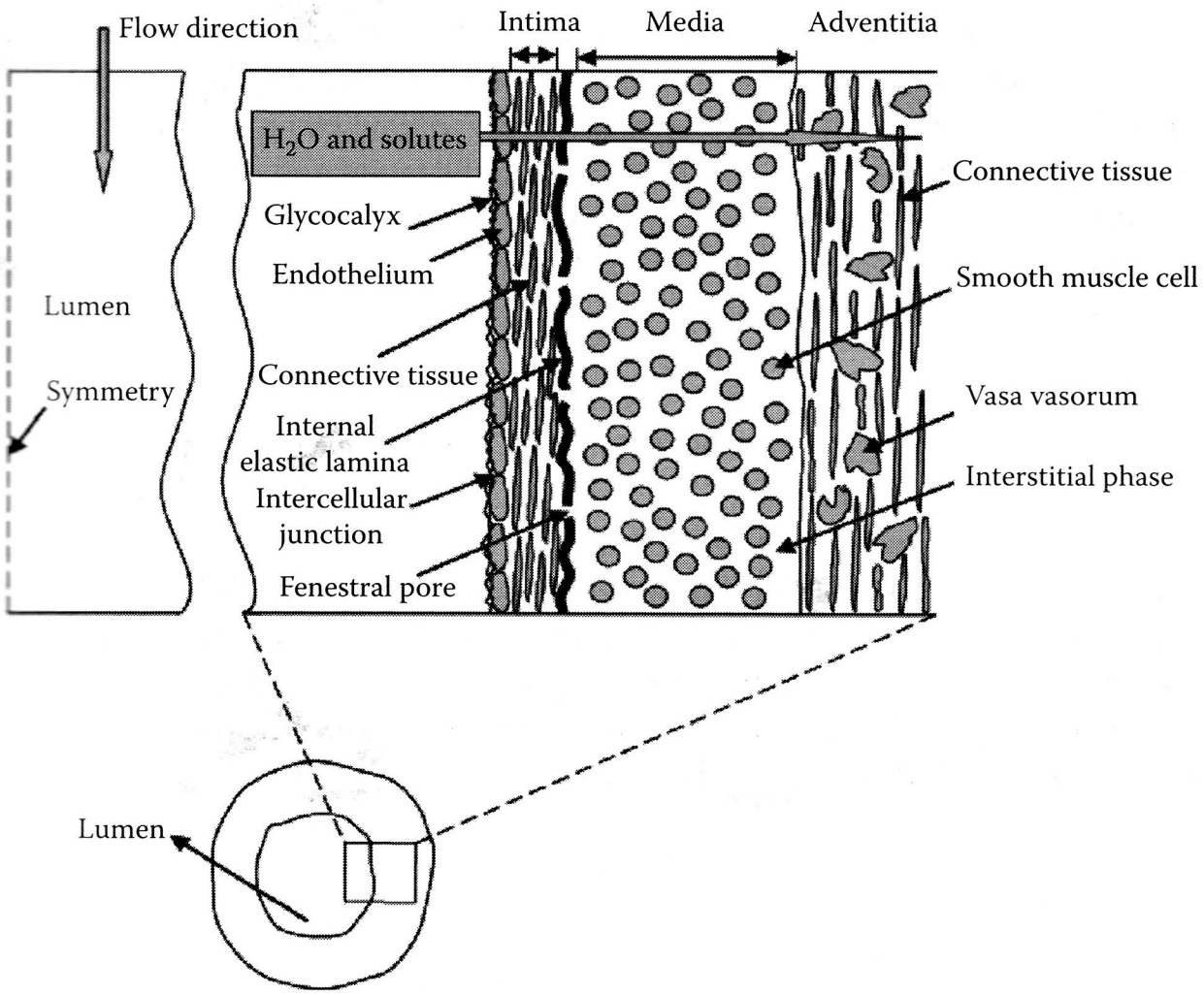

Figure 1.2 Schematic illustration of the geometric artery wall. (Reprinted from Yang and Vafai [62]. With permission from Elsevier.)

The concentration field in the arterial lumen is computed using the mass transport equation:

$$\frac{\partial c}{\partial t} + \vec{V} \cdot \nabla c = D\nabla^2 c \tag{1.38}$$

1.3.2.2 Endothelium and Internal Elastic Lamina

The endothelium and IEL were modeled as biological porous membranes [61–65]. The Staverman filtration and osmotic reflection coefficients were employed to account for selective rejection of species by the membranes and for the effects of osmotic pressure. The volume-averaged governing equations were given by

$$\nabla \cdot <\vec{V}> = 0 \tag{1.39}$$

$$\frac{\rho}{\varepsilon}\frac{\partial <\vec{V}>}{\partial t} = -\nabla <p>^f + \frac{\mu}{\varepsilon}\nabla^2 <\vec{V}> - \frac{\mu <\vec{V}>}{K} + R_u T \sigma_d \nabla <c> \tag{1.40}$$

$$\frac{\partial <c>}{\partial t} + (1-\sigma_f) <\vec{V}> \cdot \nabla <c> = D_e \nabla^2 <c> \tag{1.41}$$

where K is the permeability, and D_e is the effective macromolecule diffusivity in the medium. The symbol $<>$ denotes the local volume average of a quantity [86,87], and the superscript f refers to the local volume average inside the fluid. The parameters σ_f and σ_d are the Staverman filtration and osmotic reflection coefficients (to account for the selective permeability of biological membranes to certain solutes), respectively; T is the absolute temperature of the medium; and R_u is the universal gas constant.

1.3.2.3 Intima and Media

The intima and media were also modeled as macroscopically homogeneous porous media. Since the layers comprising the arterial wall are selectively permeable to certain species such as low-density lipoprotein (LDL), the Staverman filtration reflection coefficient has to be introduced here as well to account for this effect. The osmotic effect in the transport modeling is not included in this part since the maximum osmotic pressure gradient in the media layer is far below the hydraulic pressure gradient [88]. Therefore, the volume-averaged governing equations of the intima and media layers are as follows [61–65]:

$$\nabla \cdot <\vec{V}> = 0 \tag{1.42}$$

$$\frac{\rho}{\varepsilon}\frac{\partial <\vec{V}>}{\partial t} = -\nabla <p>^f + \frac{\mu}{\varepsilon}\nabla^2 <\vec{V}> - \frac{\mu <\vec{V}>}{K} \tag{1.43}$$

$$\frac{\partial <c>}{\partial t} + (1-\sigma_f)<\vec{V}> \cdot \nabla <c> = D_e \nabla^2 <c> + k(c) \tag{1.44}$$

where k is the effective volumetric first-order reaction rate coefficient. Table 1.4 shows various momentum equations used in modeling flow in the arterial wall. Yang and Vafai [62] presented an analytical solution for a robust four-layer porous model for description of the LDL transport in the arterial wall coupled with the transport in the lumen. The analytical results were found consistent with the numerical data for different physiological conditions, as depicted in Figures 1.3 and 1.4.

1.4 CONCLUSIONS

Most of the previous studies in the literature have assumed rigid walls for the arteries, Newtonian blood flow, and steady flow when analyzing flow and heat transfer characteristics in human tissues. Proper analysis of the arterial wall is critical in accurate modeling of arterial transport. This must be done through the use of a multilayer model that accounts for various physical attributes of the vessel and interfacial aspects between the layers. The multilayer model describes the arterial anatomy most accurately. In this model, the arterial wall is composed

Table 1.4 Momentum Equations Using the Modeling Flow in the Arterial Wall

Model	Remarks
$\vec{V} - \nabla \cdot \left(\frac{K}{\mu} P \right) = 0$	Arterial wall modeled as single-layer porous medium Darcy model Constant permeability
$\frac{\partial \vec{V}}{\partial t} + \vec{V} \cdot \nabla \vec{V} = -\frac{1}{\rho} \nabla P + \nu \nabla^2 \vec{V} - \frac{\nu \vec{V}}{K}$	Arterial wall modeled as single-layer porous medium Brinkman's model Constant permeability Neglect the Staverman filtration and osmotic reflection coefficients
$\frac{\rho}{\varepsilon} \frac{\partial <\vec{V}>}{\partial t} = -\nabla <p>^f + \frac{\mu}{\varepsilon} \nabla^2 <\vec{V}> - \frac{\mu <\vec{V}>}{K} + R_u T \sigma_d \nabla <c>$	Endothelium and internal elastic lamina More realistic The osmotic reflection coefficients were employed to account for selective rejection of species by the membranes and for the effects of osmotic pressure
$\frac{\rho}{\varepsilon} \frac{\partial <\vec{V}>}{\partial t} = -\nabla <p>^f + \frac{\mu}{\varepsilon} \nabla^2 <\vec{V}> - \frac{\mu <\vec{V}>}{K}$	Intima and media More realistic Neglects the osmotic effect in the transport modeling

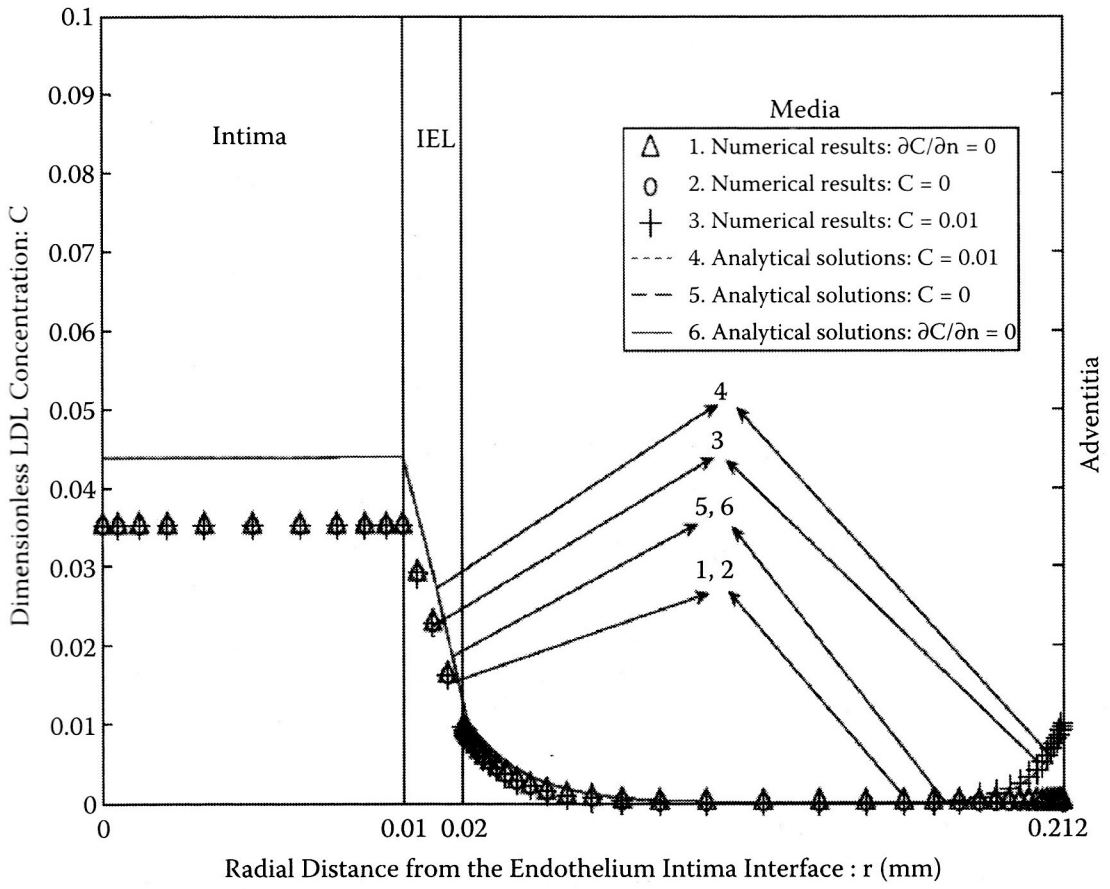

Figure 1.3 Calculated species profiles across the intima, IEL, and media layers. (Reprinted from Yang and Vafai [62]. With permission from Elsevier.)

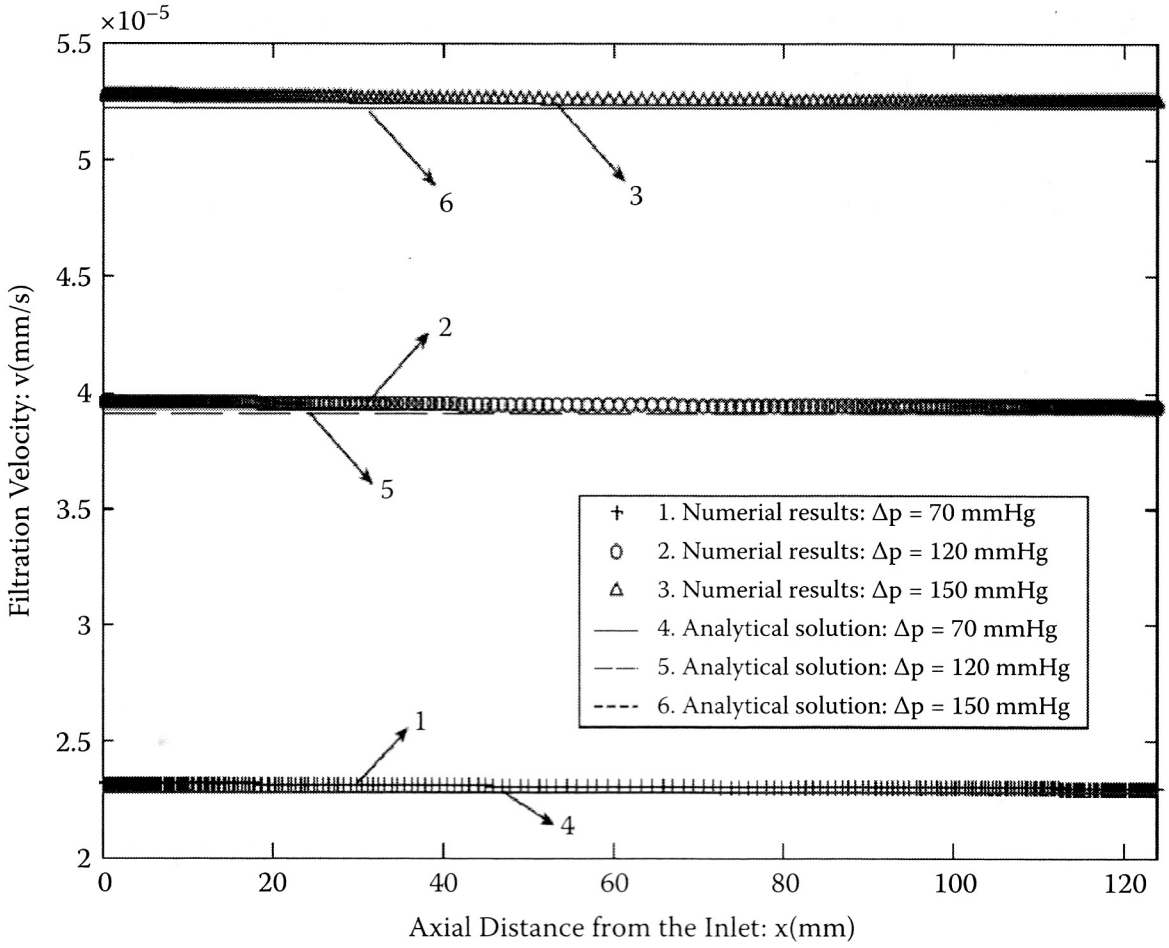

Figure 1.4 Calculated filtration velocity profiles at the lumen endothelium interface along the axial direction. (Reprinted from Yang and Vafai [62]. With permission from Elsevier.)

of four porous layers with different physiological characteristics. The multilayer model requires a number of transport parameters (properties) for each layer and in return provides an accurate profile for macromolecule distribution across the arterial wall, illuminating the role and behavior of each porous layer in the transport of macromolecules across the arterial wall. Another important factor in the accurate modeling of arterial transport is the use of a proper set of governing equations that take into account the dominant processes involved in the transport phenomenon. The Staverman filtration and osmotic reflection coefficients must be included to account for the selective rejection of species by the endothelium and IEL porous membranes as well as the effects of osmotic pressure.

The interaction between blood flow and wall can involve a wide range of fluid-mechanical phenomena. When blood flows through the lumen, the flow may deform the arterial walls and consequently alter the properties of the wall, which in turn affect flow and heat transfer characteristics in the lumen and arterial wall. Also, it will be beneficent to consider variations in the porosity and permeability of an arterial wall in future studies. In addition, the variations in the physical properties of the arterial walls such as Young's modulus and Poisson's ratio can be considered in future studies since the materials of the walls are

nonlinear and nonhomogeneous. However, these variations at this time cannot be properly described due to lack of pertinent data. For an accurate analysis of heat transfer during a hyperthermia procedure in the treatment of fetal diseases such as tumors, the porous media approach is highly recommended in order to deliver the required amount of heat source to the target volume of cancer without destroying the surrounding healthy tissues. This is because the porous media approach takes into account many pertinent effects that were neglected or simplified in the existing bioheat equations. Therefore, the mathematical models based on the porous media approach presented in the previous section are applicable in various biomedical applications such as laser eye surgery.

NOMENCLATURE

a: radius
c: concentration
c_b: blood-specific heat
c_p: tissue-specific heat
c_s: solid-specific heat
D_e: effective macromolecule diffusivity in the medium
g: perfusion bleed-off per unit vessel surface area
ΔH_f: specific enthalpy of the metabolic reaction
h_b: specific enthalpy of the blood
h_{bs}: interstitial convective heat transfer coefficient
K: permeability
$\mathbf{k}_b^a$: blood effective thermal conductivity tensor
k_{eff}: effective thermal conductivity
$\mathbf{k}_s^a$: solid-tissue effective thermal conductivity tensor
k_t: tissue thermal conductivity
n: number of arteries or veins
P: system pressure
Pe: Peclet number
q_a: heat loss from the artery by conduction through its wall
q_k: heat transfer by conduction per unit volume
q_m: rate of metabolic heat generation in the tissue layer per unit volume
q_p: heat transfer from the blood to the tissue
q_v: heat gain by conduction per unit length through the vein wall into the vein
R_u: universal gas constant
$T_{a,in}$: temperature of the blood entering the tissue
T_a^*: blood temperature in the vascular space
T_b: temperature of blood
$<T>^b$: local volume-averaged arterial blood temperature

T_o: reference temperature
T_s: solid temperature
$<T>^s$: local volume-averaged solid tissue temperature
T_t: tissue temperature
$T_{v,out}$: temperature of the blood leaving the tissue
$<\vec{V}>^b$: blood velocity vector
v_h: local mean blood velocity
v_p: mean perfusion velocity

GREEK SYMBOLS

ρ: tissue density
ρ_b: blood density
ρ_s: solid-tissue density
ω: volumetric rate of blood perfusion in the tissue per unit volume
ω^*: total perfusion bleed-off to the tissue only from the microvessels
ϕ: extent of reaction
ε: porosity
σ: geometrical factor
σ_f: osmotic reflection
σ_d: Staverman filtration

REFERENCES

1. J. Overgaard, D. G. Gonzales, M. C. Hulshof, G. Arcangeli, O. Dahl, O. Mella, and S. M. Bentzen, Hyperthermia as an Adjuvant to Radiation Therapy of Recurrent or Metastatic Melanoma: A Multicenter Randomized Trial by the European Society for Hyperthermic Oncology, *Int. J. Hypertherm.* vol. 12, pp. 3–20, 1996.
2. J. R. Oleson, D. A. Sim, and M. R. Manning, Analysis of Prognostic Variables in Hyperthermia Treatment of 161 Patients, *Int. J. Radiat. Oncol. Biol. Phys.* vol. 10, pp. 2231–2239, 1994.
3. M. W. Dewhirst and T. V. Samulski, *Hyperthermia in the Treatment for Cancer*, Kalamazoo, MI: Upjohn, 1988.
4. S. B. Field and J. W. Hand, *An Introduction to the Practical Aspects of Hyperthermia*, New York: Taylor & Francis, 1990.
5. V. Muralidharan, C. Malcontenti-Wilson, and C. Cristophi, Interstitial Laser Hyperthermia for Colorectal Liver Metastases: The Effect of Thermal Sensitization and the Use of a Cylindrical Diffuser Tip on Tumor Necrosis, *J. Clin. Laser Med. Surg.* vol. 20, pp. 189–196, 2002.
6. E. J. Hall and L. Roizin-Towle, Biological Effects of Heat, *Cancer Res.* vol. 44, pp. 4708s–4713s, 1984.
7. C. Streffer, Biological Basis for the Use of Hyperthermia in Tumor Therapy, *Strahlentherapie und Onkologie* vol. 163, pp. 416–419, 1987.
8. J. Crezee and J. W. Lagendijk, Temperature Uniformity during Hyperthermia: The Impact of Large Vessels, *Phys. Med. Biol.* vol. 37, pp. 1321–1337, 1992.

9. C. M. Beacco, S. R. Mordon, and J. M. Bruneaud, Development and Experimental in Vivo Validation of Mathematical Modeling of Laser Coagulation, *Las. Surg. Med.* vol. 14, pp. 362–373, 1994.
10. J. W. Baish, Formulation of a Statistical Model of Heat Transfer in Perfused Tissue, *J. Biomech. Engin.* vol. 116, pp. 521–527, 1994.
11. D. E. Lemons, S. Chien, L. I. Crawshaw, S. Weinbaum, and L. M. Jiji, Significance of Vessel Size and Type in Vascular Heat Transfer, *Am. J. Physiol.* vol. 253, pp. R128–R135, 1987.
12. W. Levin, M. D. Shem, B. Cooper, R. E. Hill, J. W. Hunt, and E. F. Liu, The Effect of Vascular Occlusion on Tumor Temperatures during Superficial Hyperthermia, *Int. J. Hyperthermia* vol. 10, pp. 495–505, 1994.
13. R. B. Roemer, The Local Tissue Cooling Coefficient: A Unified Approach to Thermal Washout and Steady-State Perfusion Calculations, *Int. J. Hyperthermia* vol. 6, pp. 421–430, 1990.
14. M. C. Kolios, M. D. Sherar, and J. W. Hunt, Large Blood Vessel Cooling in Heated Tissues: A Numerical Study, *Phys. Med. Biol.* vol. 40, pp. 477–494, 1995.
15. M. C. Kolios, A. E. Worthington, D. W. Holdsworth, M. D. Sherar, and J. W. Hunt, An Investigation of the Flow Dependence of Temperature Gradients near Large Vessels during Steady State and Transient Tissue Heating, *Phys. Med. Biol.* vol. 44, pp. 1479–1497, 1999.
16. X. Tang, W. Dai, R. Nassar, and A. Bejan, Optimal Temperature Distribution in a Three-Dimensional Triple-Layered Skin Structure Embedded with Artery and Vein Vasculature, *Num. Heat Trans.: Pt. A: Appl.* vol. 50, pp. 809–834, 2006.
17. W. Dai, A. Bejan, X. Tang, L. Zhang, and R. Nassar, Optimal Temperature Distribution in a Three Dimensional Triple-Layered Skin Structure with Embedded Vasculature, *J. Appl. Phys.* vol. 99(104702), pp. 809–834, 2006.
18. Y. He, M. Shirazaki, H. Liu, R. Himeno, and Z. Sun, A Numerical Coupling Model to Analyze the Blood Flow, Temperature, and Oxygen Transport in Human Breast Tumor under Laser Irradiation, *Comp. Biol. Med.* vol. 36, pp. 1336–1350, 2006.
19. T. C. Shih, H. L. Liu, and A. Horng, Cooling Effect of Thermally Significant Blood Vessels in Perfused Tumor Tissue during Thermal Therapy, *Int. Commun. Heat Mass Trans.* vol. 33, pp. 135–141, 2006.
20. J. Zhou and J. Liu, Numerical Study on 3-D Light and Heat Transport in Biological Tissues Embedded with Large Blood Vessels during Laser-Induced Thermotherapy, *Numer. Heat Trans. A* vol. 45, pp. 415–449, 2004.
21. K. M. Khanafer, J. L. Bull, I. Pop, and R. Berguer, Influence of Pulsatile Blood Flow and Heating Scheme on the Temperature Distribution during Hyperthermia Treatment, *Int. J. Heat Mass Trans.* vol. 50, pp. 4883–4890, 2007.
22. O. I. Craciunescu and C. T. Clegg, Pulsatile Blood Flow Effects on Temperature Distribution and Heat Transfer in Rigid Vessels, *ASME J. Biomech. Engin.* vol. 123, pp. 500–505, 2001.
23. K. R. Diller, in Y. I. Cho, Editor, *Advances in Heat Transfer: Bioengineering Heat Transfer*, New York: Academic Press, 1992.
24. J. Voke, Lasers and Their Use in Ophthalmology, *Optom. Today: Pt. 3*, pp. 31–36, June 2001.
25. C. Purslow and J. Wolffsohn, Ocular Surface Temperature: A Review, *Eye Cont. Lens* vol. 31, pp. 117–123, 2005.
26. E. H. Ooi, W. T. Ang, and E. Y. K. Ng, Bioheat Transfer in the Human Eye: A Boundary Element Approach, *Engin. Anal. Bound. Elem.* vol. 31, pp. 494–500, 2007.
27. E. Y. K. Ng and E. H. Ooi, FEM Simulation of the Eye Structure with Bioheat Analysis, *Comp. Met. Prog. Biomed.* vol. 82, pp. 268–276, 2006.

28. E. Y. K. Ng and E. H. Ooi, Ocular Surface Temperature: A 3D FEM Prediction Using Bioheat Equation, *Comp. Biol. Med.* vol. 37, pp. 829–835, 2007.
29. J. A. Scott, A Finite Element Model of Heat Transport in the Human Eye, *Phys. Med. Biol.* vol. 33, pp. 227–242, 1988.
30. K. J. Chuak, J. C. Ho, S. K. Chou, and M. R. Islam, The Study of the Temperature Distribution within a Human Eye Subjected to a Laser Source, *Int. Commun. Heat Mass Trans.* vol. 32, pp. 1057–1065, 2005.
31. E. H. Amara, Numerical Investigations on Thermal Effects of Laser-Ocular Media Interaction, *Int. J. Heat Mass Trans.* vol. 38, pp. 2479–2488, 1995.
32. J. A. Scott, The Computation of Temperature Rises in the Human Eye Induced by Infrared Radiation, *Phys. Med. Biol.* vol. 33, pp. 243–257, 1988.
33. A. Hirata, Temperature Increase in Human Eyes Due to Near-Field and Far-Field Exposures at 900 MHz, 1.5 GHz and 1.9 GHz, *IEEE Trans. Electromagn. Compat.* vol. 47, pp. 68–76, 2005.
34. A. Hirata, S. Matsuyama, and T. Shiozawa, Temperature Rises in the Human Eye Exposure to EM Waves in the Frequency Range 0.6–6 GHz, *IEEE Trans. Electromagn. Compat.* vol. 42, pp. 386–393, 2000.
35. A. Hirata, S. Watanabe, M. Kojima, I. Hata, K. Wake, M. Taki, K. Sasaki, O. Fujiwara, and T. Shiozawa, Computational Verification of Anesthesia Effect on Temperature Variations in Rabbit Eyes Exposed to 2.45 GHz Microwave Energy, *Bioelectromagnetics* vol. 27, pp. 602–612, 2006.
36. J. J. W. Lagendijk, A Mathematical Model to Calculate Temperature Distributions in Human and Rabbit Eyes during Hyperthermic Treatment, *Phys. Med. Biol.* vol. 27, pp. 1301–1311, 1982.
37. H. H. Pennes, Analysis of Tissue and Arterial Blood Temperature in the Resting Human Forearm, *J. Appl. Phys.* vol. 1, pp. 93–122, 1948.
38. C. K. Charny, Mathematical Models of Bioheat Transfer, *Adv. Heat Trans.* vol. 22, pp. 19–152, 1992.
39. H. Arkin, L. X. Xu, and K. R. Holmes, Recent Developments in Modeling Heat Transfer in Blood Perfused Tissues, *IEEE Trans. Biomed. Engin.* vol. 41, pp. 97–107, 1994.
40. T. W. McGrail and R. C. Seagrave, Application of the Bioheat Transfer Equation in Fetal-Placental Studies, *Annals N.Y. Acad. Sci.* vol. 335, pp. 161–172, 1980.
41. C. Wood and R. W. Beard, Temperature of the Human Fetus, *J. Obstet. Gynec. Brit. Commun.* vol. 71, pp. 768–769, 1964.
42. K. Adamsonsk and M. E. Towell, Thermal Homeostasis in the Fetus and Newborn, *Anesthesiology* vol. 26, pp. 531–540, 1965.
43. F. M. Hart and J. J. Faber, Fetal and Maternal Temperatures in Rabbits, *J. Appl. Phys.* vol. 20, pp. 737–741, 1965.
44. D. Walker, A. Walker, and C. Wood, Temperature of the Human Fetus, *J. Obstet. Gynec. Brit. Commun.* vol. 76, pp. 503–511, 1969.
45. D. Abramsr, D. Caton, L. B. Curetc, C. Crenshaw, L. Mann, and D. Barron, Fetal Brain-Maternal Aorta-Temperature Differences in Sheep, *Am. J. Physiol.* vol. 217, pp. 1619–1622, 1969.
46. D. Abramsr, D. Caton, J. Clapp, and D. Barron, Thermal and Metabolic Features of Life in Utero, *Clin. Obstet. Gynec.* vol. 13, pp. 549–564, 1970.
47. D. Poljak, A. Peratta, and C. Brebbia, The Boundary Element Electromagnetic-Thermal Analysis of Human Exposure to Base Station Antennas Radiation, *Engin. Anal. Bound. Elem.* vol. 28, pp. 763–770, 2004.

48. C. K. Charny and R. L. Levin, Heat Transfer Normal to Paired Arteries and Veins Embedded in Perfused Tissue during Hyperthermia, *Trans. ASME J. Biomech. Engin.* vol. 110, pp. 277–282, 1988.
49. C. K. Charny and R. L. Levin, Bioheat Transfer in a Branching Countercurrent Net-work during Hyperthermia, *ASME J. Biomech. Engin.* vol. 111, pp. 263–270, 1989.
50. R. B. Roemer and T. C. Cetas, Applications of Bioheat Transfer Simulations in Hyperthermia, *Cancer Res.* vol. 44, pp. 4788–4798, 1984.
51. W. Wulff, The Energy Conservation Equation for Living Tissues, *IEEE Trans. Biomed. Engin.* vol. 21, pp. 494–495, 1974.
52. H. G. Klinger, Heat Transfer in Perfused Tissue—I: General Theory, *Bull. Math. Biol.* vol. 36, pp. 403–415, 1974.
53. M. M. Chen and K. R. Holmes, Microvascular Contributions in Tissue Heat Transfer, *Annals N.Y. Acad. Sci.* vol. 335, pp. 137–150, 1980.
54. S. Weinbaum and L. M. Jiji, A Two Phase Theory for the Influence of Circulation on the Heat Transfer in Surface Tissue, in M. K. Wells, Editor, *Advances in Bioengineering*, pp. 179–182, New York: ASME, 1979.
55. S. Weinbaum, L. M. Jiji, and D. E. Lemons, Theory and Experiment for the Effect of Vascular Microstructure on Surface Tissue Heat Transfer: Part I: Anatomical Foundation and Model Conceptualization, *ASME J. Biomech. Engin.* vol. 106, pp. 321–330, 1984.
56. S. Weinbaum, L. M. Jiji, and D. E. Lemons, Theory and Experiment for the Effect of Vascular Microstructure on Surface Tissue Heat Transfer: Part II: Model Formulation and Solution, *ASME J. Biomech. Engin.* vol. 106, pp. 331–341, 1984.
57. S. Weinbaum and L. M. Jiji, A New Simplified Equation for the Effect of Blood Flow on Local Average Tissue Temperature, *ASME J. Biomech. Engin.* vol. 107, pp. 131–139, 1985.
58. A. Bejan, I. Dincer, S. Lorente, A. Miguel, and A. Reis, *Porous and Complex Flow Structures in Modern Technologies*, New York: Springer-Verlag, 2004.
59. K. Khanafer and K. Vafai, The Role of Porous Media in Biomedical Engineering as Related to Magnetic Resonance Imaging and Drug Delivery, *Heat Mass Trans.* vol. 42, pp. 939–953, 2006.
60. A.-R. A. Khaled and K. Vafai, The Role of Porous Media in Modeling Flow and Heat Transfer in Biological Tissues, *Int. J. Heat Mass Trans.* vol. 46, pp. 4989–5003, 2003.
61. L. Ai and K. Vafai, A Coupling Model for Macromolecule Transport in a Stenosed Arterial Wall, *Int. J. Heat Mass Trans.* vol. 49, pp. 1568–1591, 2006.
62. N. Yang and K. Vafai, Low Density Lipoprotein (LDL) Transport in an Artery: A Simplified Analytical Solution, *Int. J. Heat Mass Trans.* vol. 51, pp. 497–505, 2008.
63. M. Khakpour and K. Vafai, A Critical Assessment of Arterial Transport Models, *Int. J. Heat Mass Trans.* vol. 51, pp. 807–822, 2008.
64. M. Khakpour and K. Vafai, A Complete Analytical Solution for Mass Transport within a Multilayer Arterial Wall, *Int. J. Heat Mass Trans.* vol. 51, pp. 2905–2913, 2008.
65. K. Khanafer, A. R. A. Khaled, and K. Vafai, Spatial Optimization of an Array of Aligned Microcantilever Biosensors, *J. Micromech. Microengin.* vol. 14, pp. 1328–1336, 2004.
66. A. R. A. Khaled and K. Vafai, Optimization Modeling of Analyte Adhesion over an Inclined Microcantilever-Based Biosensor, *J. Micromech. Microengin.* vol. 14, pp. 1220–1229, 2004.

67. A. R. A. Khaled and K. Vafai, Analysis of Oscillatory Flow Disturbances and Thermal Characteristics inside Fluidic Cells Due to Fluid Leakage and Wall Slip Conditions, *J. Biomech.* vol. 3, pp. 721–729, 2004.
68. K. Khanafer and K. Vafai, Geometrical and Flow Configurations for Enhanced Microcantilever Detection within a Fluidic Cell, *Int. J. Heat Mass Trans.* vol. 48, pp. 2886–2895, 2005.
69. K. Vafai, *Handbook of Porous Media*, New York: Marcel Dekker, 2000.
70. K. Vafai, *Handbook of Porous Media*, 2nd ed., New York: Taylor & Francis Group, 2005.
71. H. Hadim and K. Vafai, Overview of Current Computational Studies of Heat Transfer in Porous Media and Their Applications: Forced Convection and Multiphase Transport, *Adv. Numer. Heat Trans.* vol. 2, pp. 291–330, 2000.
72. K. Vafai and H. Hadim, Overview of Current Computational Studies of Heat Transfer in Porous Media and Their Applications: Natural Convection and Mixed Convection, *Adv. Numer. Heat Trans.* vol. 2, pp. 331–371, 2000.
73. Y. M. Xuan and W. Roetzel, Bioheat Equation of the Human Thermal System, *Chem. Eng. Technol.* vol. 20, pp. 268–276, 1997.
74. Y. M. Xuan and W. Roetzel, Transfer Response of the Human Limb to an External Stimulus, *Int. J. Heat Mass Trans.* vol. 41, pp. 229–239, 1998.
75. A. Amiri and K. Vafai, Analysis of Dispersion Effects and Nonthermal Equilibrium, Non-Darcian, Variable Porosity Incompressible-Flow through Porous Media, *Int. J. Heat Mass Trans.* vol. 37, pp. 939–954, 1994.
76. A. Amiri and K. Vafai, Transient Analysis of Incompressible Flow through a Packed Bed, *Int. J. Heat Mass Trans.* vol. 41, pp. 4259–4279, 1998.
77. B. Alazmi and K. Vafai, Constant Wall Heat Flux Boundary Conditions in Porous Media under Local Thermal Non-Equilibrium Conditions, *Int. J. Heat Mass Trans.* vol. 45, pp. 3071–3087, 2002.
78. D. Y. Lee and K. Vafai, Analytical Characterization and Conceptual Assessment of Solid and Fluid Temperature Differentials in Porous Media, *Int. J. Mass Trans.* vol. 42, pp. 423–435, 1999.
79. K. Vafai and M. Sozen, Analysis of Energy and Momentum Transport for Fluid Flow through a Porous Bed, *ASME J. Heat Trans.* vol. 112, pp. 690–699, 1990.
80. K. Vafai and M. Sozen, An Investigation of a Latent Heat Storage Packed Bed and Condensing Flow through It, *ASME J. Heat Trans.* vol. 112, pp. 1014–1022, 1990.
81. K. Vafai and M. Sozen, A Comparative Analysis of Multiphase Transport Models in Porous Media, *Ann. Rev. Heat Trans.* vol. 3, pp. 145–162, 1990.
82. M. Sozen and K. Vafai, Analysis of Oscillating Compressible Flow through a Packed Bed, *Int. J. Heat Fluid Flow* vol. 12, pp. 130–136, 1991.
83. M. Sozen and K. Vafai, Analysis of the Non-Thermal Equilibrium Condensing Flow of a Gas through a Packed Bed, *Int. J. Heat Mass Trans.* vol. 33, pp. 1247–1261, 1990.
84. A. Marafie and K. Vafai, Analysis of Non-Darcian Effects on Temperature Differentials in Porous Media, *Int. J. Heat Mass Trans.* vol. 44, pp. 4401–4411, 2001.
85. K. Vafai and C. L. Tien, Boundary and Inertia Effects on Convective Mass Transfer in Porous Media, *Int. J. Heat Mass Trans.* vol. 25, pp. 1183–1190, 1981.
86. K. Vafai and C. L. Tien, Boundary and Inertia Effects on Flow and Heat Transfer in Porous Media, *Int. J. Heat Mass Trans.* vol. 24, pp. 195–203, 1980.
87. Z. J. Huang and J. M. Tarbell, Numerical Simulation of Mass Transfer in Porous Media of Blood Vessel Walls, *Am. J. Physiol.* vol. 273, pp. H464–H477, 1997.